Utility of ^{18}F-FDG PET/CT in the Assessment of Lymphoepithelioma-like Carcinoma

Objective: Lymphoepithelioma-like carcinoma (LELC) is a rare Epstein-Barr virus (EBV)-related disease, which commonly originates from the lung and is associated with more favourable treatment outcomes compared to other non-LELC thoracic carcinomas. Radiological assessment utilizing ^{18}Fluorine-fluorodeoxyglucose positron emission tomography combined with computed tomography (^{18}F-FDG PET/CT) is important for initial disease staging to tailor the treatment strategy, evaluation of treatment response and detection of disease recurrence. The purpose of this article was to highlight the utility of ^{18}F-FDG PET/CT in different stages of disease evaluation of LELC.
Methods: We reviewed 7 patients with histologically proven LELC who underwent ^{18}F-FDG PET/CT for disease evaluation.
Results: We described the ^{18}F-FDG avidity of LELC (ranged from SUVmax 7.6 to SUVmax 14.5 in our series) and highlighted the clinical values of ^{18}F-FDG PET/CT in different stages of disease evaluation. ^{18}F-FDG PET/CT allows accurate evaluation of the primary tumour, its relationship with the surrounding structures and accurate staging. It is also useful in treatment response assessment to monitor the efficacy of the treatment and to decide upon treatment strategy. Given the ^{18}F-FDG avidity of LELC, ^{18}F-FDG PET/CT is advantageous in detecting tumour recurrence of LELC.
Conclusion: LELC is a rare disease entity associated with EBV and is more prevalent in Asia, where EBV is endemic. LELC is FDG-avid tumour. Although the features on ^{18}F-FDG PET/CT are not specific, ^{18}FDG PET/CT offers valuable information on disease management of LELC.

Key words: ^{18}F-FDG PET/CT; ^{18}FDG; lymphoepithelioma-like carcinoma; LELC; SUV

Introduction

Begin and associates first reported lymphoepithelioma-like carcinoma (LELC) in 1987 [1]. More than 150 cases were reported until 2006 [2]. The commonest site of primary tumour is the lung but LELC has also been reported in salivary glands, thymus, stomach, urogenital system and skin. LELC is closely associated with Epstein-Barr virus (EBV) infection and mostly seen in Asia with nearly two-thirds of the reported cases found in Taiwan, Southern China, and Hong Kong [3].

On histology, LELC is similar to undifferentiated nasopharyngeal carcinoma (NPC). The tumour cells are arranged in nests or sheets with intense lymphoplasmacytic cell infiltration. The cell borders are ill-defined, giving rise to syncytial aggregation of tumour cells. The cell nuclei are round, oval, or elongated, with mildly irregular nuclear borders, clumped

chromatin, and 1 or 2 distinct eosinophilic nucleoli. Association with EBV is observed mainly in LELC arising in the Asian population, which can be demonstrated by serologic, immunohistochemical, nucleic acid detection and in-situ hybridization techniques. In-situ hybridization using a sensitive digoxigenin-labelled RNA probe is the most commonly employed detection method for EBV- encoded small RNAs (EBER) [4]. Patchy expression of the viral latent membrane protein (LMP-1) can be demonstrated using immunohistochemistry [4]. In cancers that morphologically resemble LELC but which arise in Caucasians or in other organs such as skin, vagina and urinary bladder are not associated with EBV infection [3].

The most common type of LELC, pulmonary LELC, accounts for 0.9% of bronchogenic carcinoma [5]. The prognosis of pulmonary LELC is better compared to other non-LELC lung carcinoma; the 2-year and 5-year overall survival rates for pulmonary LELC were reported as 79.9% and 53.5% as compared to non-LELC lung carcinoma, which were lower at 59.5% and 39.1% respectively [3]. It is also indistinguishable from the metastasis originated from NPC. Therefore, nasopharyngeal origin needs to be excluded in all cases. According to WHO histological classification of lung tumours, pulmonary LELC belongs to a subtype of variants of large cell carcinoma [3].

This article aimed to demonstrate the potential roles of ^{18}F-FDG PET/CT in the assessment of LELC from initial disease detection to surveillance; allowing global reflection of metabolic active tumour burden in assisting treatment stratification and clinical management.

Methods

Seven cases selected for this atlas article were collected between November 2007 and April 2015. All selected cases were histologically confirmed cases of LELC. There were 4 pulmonary LELC and 3 non-pulmonary LELC. All examinations were performed using dedicated PET/CT scanner (Discovery VCT, 64-multislice CT, GE Healthcare Bio-Sciences Corp.), covering from the skull base to the upper thighs. Patients were required to fast for 6 hours before the examination and the serum glucose was ensure not to exceed 180mg/dl before injecting 10mCi (370MBq) ^{18}F-FDG. Image acquisition started at 60 minutes after ^{18}F-FDG injection. PET images were reconstructed using an ordered-subset expectation maximization iterative algorithm (14 subsets and two iterations) and CT was used for attenuation correction of the PET emission data. An experienced radiologist with 4 years experience in PET and more than 8 years experience in CT reviewed all the cases.

Results and Discussion

^{18}FDG-avidity of LELC

There is few published data, limiting to case reports, in the ^{18}F-FDG-avidity of LELC [6-10]. All cases were ^{18}F-FDG-avid with wide-range of reported maximum standardized uptake values (SUVmax), ranging from SUVmax 1.7 to SUVmax 34.5 [6, 7, 9]. The previous observation concurs with our experience in these 7 patients, whom the LELC was metabolically active, with SUVmax 7.6 to SUVmax 14.5.

Primary Disease Detection

^{18}F-FDG PET/CT is able to detect primary site of LELC shortly after the development of clinical symptoms [6]. In locally advanced disease, ^{18}F-FDG PET/CT allows accurate evaluation of the extent of the primary disease, its relationship with the local structures and resectability. We present a case of a 54-year-old woman who presented with new onset of cough. A lingular mass was found on CT thorax. Bronchoscopic biopsy confirmed the mass to be poorly differentiated carcinoma with suspicious LELC features; ^{18}F-FDG PET-CT was performed for pre-operative assessment (Fig. 1). She went on to have a left pneumonectomy and LELC was confirmed. The integration of morphological and functional details allows ^{18}F-FDG PET/CT to be a more accurate imaging tool for primary disease assessment than CT or ^{18}F-FDG PET alone.

Staging

^{18}FDG PET/CT adopts a whole-body imaging coverage, allowing global evaluation of disease burden for accurate staging. Aside from the primary tumour, nodal and distant metastatic involvements are assessed. Distant organ metastases have not been previously described by other radiological studies on LELC [6, 7, 10-12]. Given the association with EBV, the nasopharynx, as included in the field of view on ^{18}F-FDG PET/CT, should be carefully scrutinized for occult NPC. This is highlighted in a 60-year-old woman with a biopsy-confirmed LELC of the posterior mediastinal mass, the histology suggested that the primary tumour could be originating from the lung, thymus or nasopharynx. She was referred for ^{18}FDG PET-CT to rule out NPC, other site of involvement and distant metastasis (Fig. 2).

Accurate staging is crucial in deciding treatment strategy. Previous study showed that pulmonary LELC had preponderance for peribronchovascular and mediastinal spread [13]; hence, precise nodal staging is paramount in pulmonary LELC. Although tissue diagnosis remains important for small volume mediastinal disease, ^{18}FDG PET/CT can aid in selecting the appropriate patients for more invasive mediastinal staging tests [14]. Surgery is the mainstay curative treatment for early stage pulmonary LELC, whereas combination therapy

including adjuvant radiotherapy, chemotherapy or chemoradiation is required for more advanced disease [2].

Treatment Response Assessment

In case of unexpected LELC, where diagnosis is made on resected specimen, post-operative ^{18}F-FDG PET/CT can provide information on residual disease and acts as baseline assessment prior to further therapy, if required. Furthermore, the changes in the ^{18}F-FDG avidity and the sizes of the tumours can be useful in monitoring treatment response in subsequent follow-up. Here, we present a 66-year old man who had previous right upper lobectomy for pulmonary LELC. He suffered from disease recurrence in January 2015 and was given 4 cycles of chemotherapy. Pre-treatment and post-treatment ^{18}FDG PET/CT scans were performed for treatment response assessment (Fig. 3). ^{18}FDG PET/CT helps to identify patient who experiences progressive disease, to spare the patient from ineffective treatment and to offer alternative therapy.

Detection of Recurrence

Tumour progression could occur after years of stable disease. A 65-year-old woman, with diagnosis of stage IV pulmonary LELC in 2007, was previously treated by radiotherapy to mediastinum, followed by 6 cycles of chemotherapy. She remained in remission until early 2010, when she complained of low back pain and pelvic pain. ^{18}FDG PET/CT was requested to detect disease recurrence (Fig. 4). Disease surveillance is important; ^{18}F-FDG PET/CT helps to differentiate tumour recurrence from benign pathology, such as that of post-treatment changes and sometimes, infective entities.

Non-pulmonary LELC

Although pulmonary LELC is the most common type of LELC, it can affect other organs. These non-pulmonary LELC, including the recurrences, are ^{18}FDG-avid in our experience.

We present a case of thymic LELC in a 53-year-old man with symptoms of superior vena cava obstruction. Staging ^{18}FDG PET/CT was performed (Fig. 5).

Next, we present a 30-year-old man with limb numbness, weakness and muscle wasting; a clinical suspicion of myasthenia gravis was suspected. CT detected a huge anterior mediastinal mass with a left liver mass. Therefore, ^{18}FDG PET/CT was subsequently requested for disease evaluation (Fig. 6). He underwent radical thymectomy, in which carcinoma of LELC variant was confirmed.

Finally, we present a 66-year-old man, who was previously treated for LELC of the parotid gland in 1997 with right parotidectomy and radiotherapy. In 2015, he represented with hepatomegaly and EBV DNA was elevated to 42375 copies/ml. ^{18}FDG PET/CT was performed to detect disease recurrence (Fig. 7).

Conclusion

LELC is a rare disease entity associated with EBV and is more prevalent in Asia, where EBV is endemic. LELC is ^{18}FDG-avid tumour. Although the features on ^{18}FDG PET/CT are not specific, ^{18}FDG PET/CT offers valuable information on disease detection, staging, treatment response evaluation and disease surveillance.

Conflict of interest

There was no conflict of interest.

References

1. Begin LR, Eskandari J, Joncas J, Panasci L. Epstein-Barr virus related lymphoepithelioma-like carcinoma of lung. *J Surg Oncol.*1987;**36**:280-283.

2. Ho JC WM, Lam WK.Ho. Lymphoepithelioma-like carcinoma of the lung. . *Respiratory.*2006;**11**:539-545.

3. Han AJ, Xiong M, Gu YY, Lin SX, Xiong M. Lymphoepithelioma-like carcinoma of the lung with a better prognosis. A clinicopathologic study of 32 cases. *Am J Clin Pathol.*2001;**115**:841-850.

4. Wong MP CL, Yuen ST, Leung SY, Chan SY, Wang E, Fu KH. In situ detection of Epstein-Barr virus in non-small cell lung carcinomas. *J Pathol.*1995J;**177**:233-240.

5. Han AJ, Xiong M, Zong YS. Association of Epstein-Barr virus with lymphoepithelioma-like carcinoma of the lung in southern China. *Am J Clin Pathol.*2000;**114**:220-226.

6. Dong A, Zhang J, Wang Y, Zhai Z, Zuo C. FDG PET/CT in primary pulmonary lymphoepithelioma-like carcinoma. *Clin Nucl Med.*2015;**40**:134-137.

7. Shen DH, Cheng CY, Lin LF, Gao HW, Cheng YL, Chen CY. Conversion from FDG-negative to -positive during follow-up in a rare case of pulmonary lymphoepithelioma-like carcinoma. *Clin Nucl Med.*2012;**37**:679-681.

8. Koppula BR, Pipavath S, Lewis DH. Epstein-Barr virus (EBV) associated lymphoepithelioma-like thymic carcinoma associated with paraneoplastic syndrome of polymyositis: a rare tumor with rare association. *Clin Nucl Med.*2009;**34**:686-688.

9. Lee SD, Chiu YL, Wu CS, Peng NJ. 18F-FDG PET/CT of Liver Lymphoepithelioma-like Carcinoma. *Clin Nucl Med.*2015;**40**:732-733.

10. Yener NA, Balikci A, Cubuk R, Midi A, Orki A, Eren Topkaya A. Primary lymphoepithelioma-like carcinoma of the lung: report of a rare case and review of the literature. *Turk Patoloji Derg.*2012;**28**:286-289.

11. Huang CJ, Chan KY, Lee MY, Hsu LH, Chu NM, Feng AC, et al. Computed tomography characteristics of primary pulmonary lymphoepithelioma-like carcinoma. *Br J Radiol.*2007;**80**:803-806.

12. Mo Y SJ, Zhang Y, Zheng L, Gao F, Liu L, Xie C. Primary lymphoepithelioma-like carcinoma of the lung: distinct computed tomography features and associated clinical outcomes. *J Thorac Imaging.*2014;**29**:246-251.

13. Ooi GC, Ho JC, Khong PL, Wong MP, Lam WK, Tsang KW. Computed tomography characteristics of advanced primary pulmonary lymphoepithelioma-like carcinoma. *Eur Radiol.*2003;**13**:522-526.

14. Detterbeck FC, Jantz MA, Wallace M, Vansteenkiste J, Silvestri GA, American College of Chest P. Invasive mediastinal staging of lung cancer: ACCP evidence-based clinical practice guidelines (2nd edition). *Chest.*2007;**132**:202S-220S.

Legends

Fig. 1

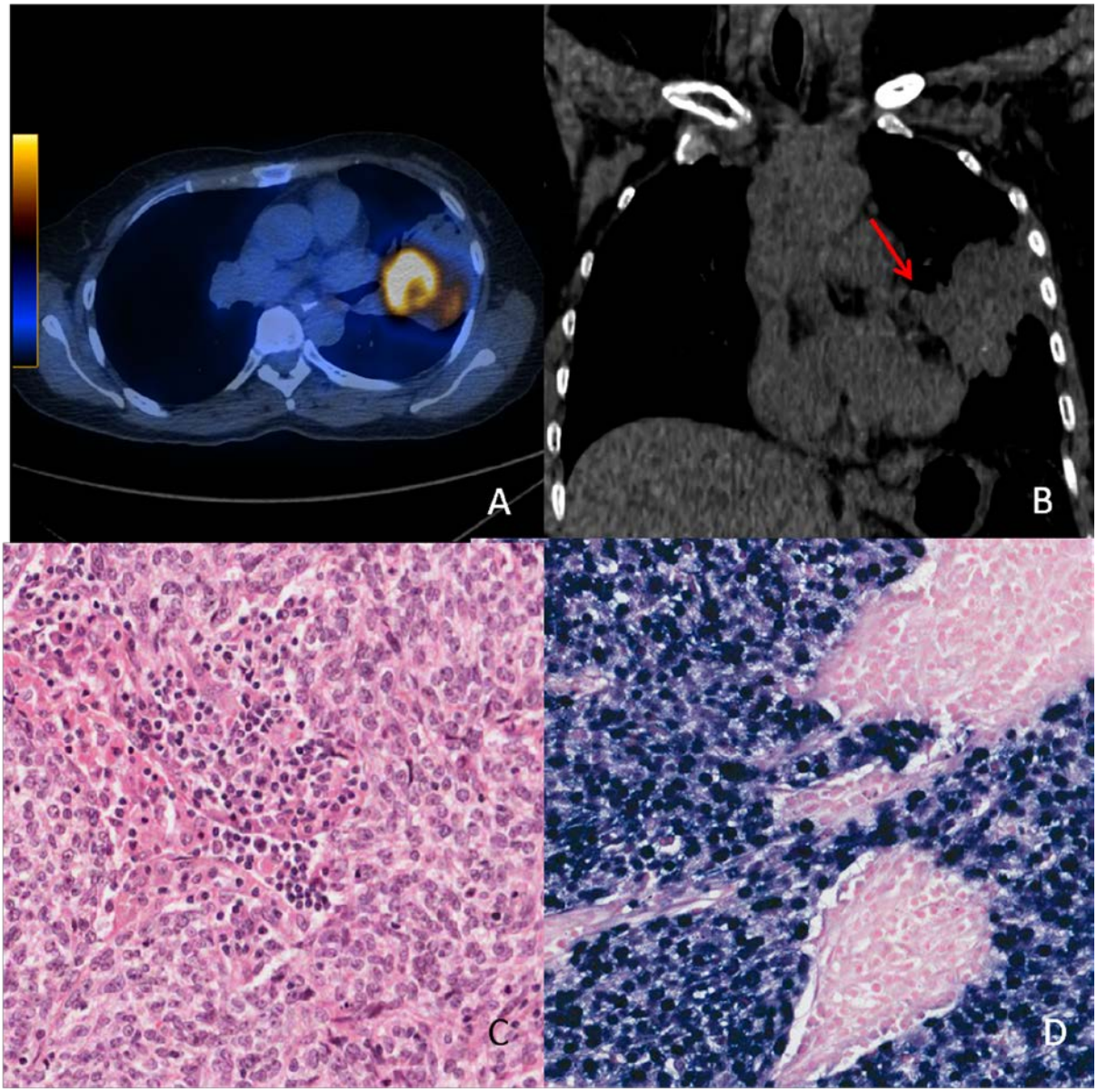

(A) Axial fused ^{18}FDG PET/CT image shows a hypermetabolic lung mass extending from the left hilum to involve the apico-posterior segment of the left upper lobe, measuring 7.9 x 6.2 cm with SUVmax 7.6, suggestive of primary lung carcinoma.

(B) Coronal CT image shows the primary lung tumour infiltrating into the mediastinal fat, suggestive of early mediastinal invasion (arrow).

(C) Hematoxylin and eosin section of LELC showing sheets of undifferentiated tumour cells admixed with abundant lymphoplasmacytic infiltrate (original magnification x 200).

(D) In-situ hybridization with EBV- encoded small RNAs (EBER) probes showing diffuse strong nuclear signals (blue) in all tumour cells and absence of signals of surrounding stroma and inflammatory cells (original magnification x 200).

Fig. 2

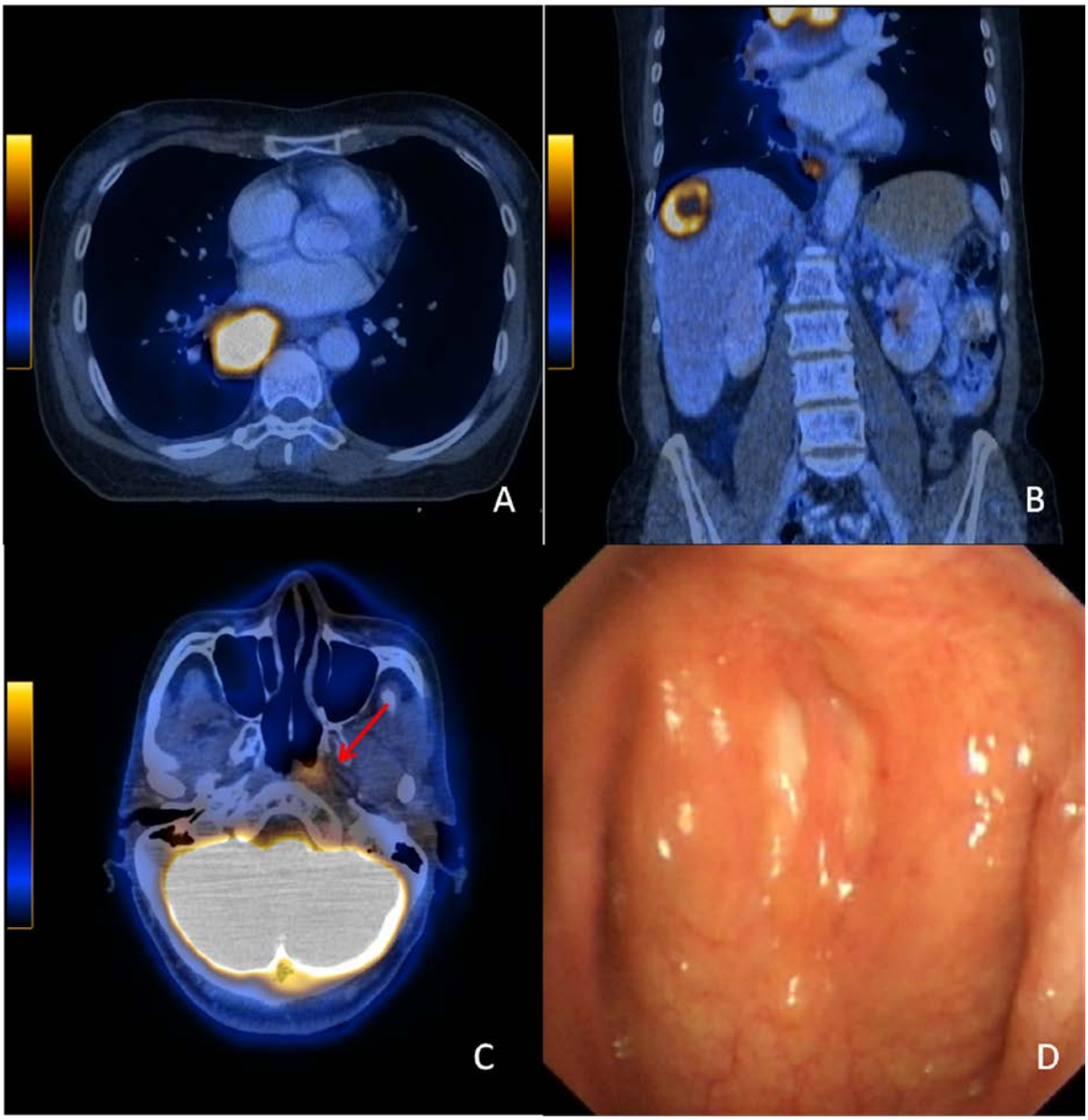

(A) Axial fused ^{18}FDG PET/CT image shows a hypermetabolic right posterior mediastinal mass (SUVmax 14.1).
(B) Coronal fused ^{18}FDG PET/CT image shows a hypermetabolic hepatic metastasis in segment 7 / 8 with central necrosis.
(C) Axial fused ^{18}FDG PET/CT image shows asymmetrical ^{18}FDG uptake at the left nasopharynx with mild mucosal thickening (arrow).
(D) Nasal endoscopy reveals irregular mucosal corresponding to the left nasopharynx uptake. Subsequent biopsy result was negative for malignancy, ruling out the presence of nasopharyngeal carcinoma.

Fig. 3

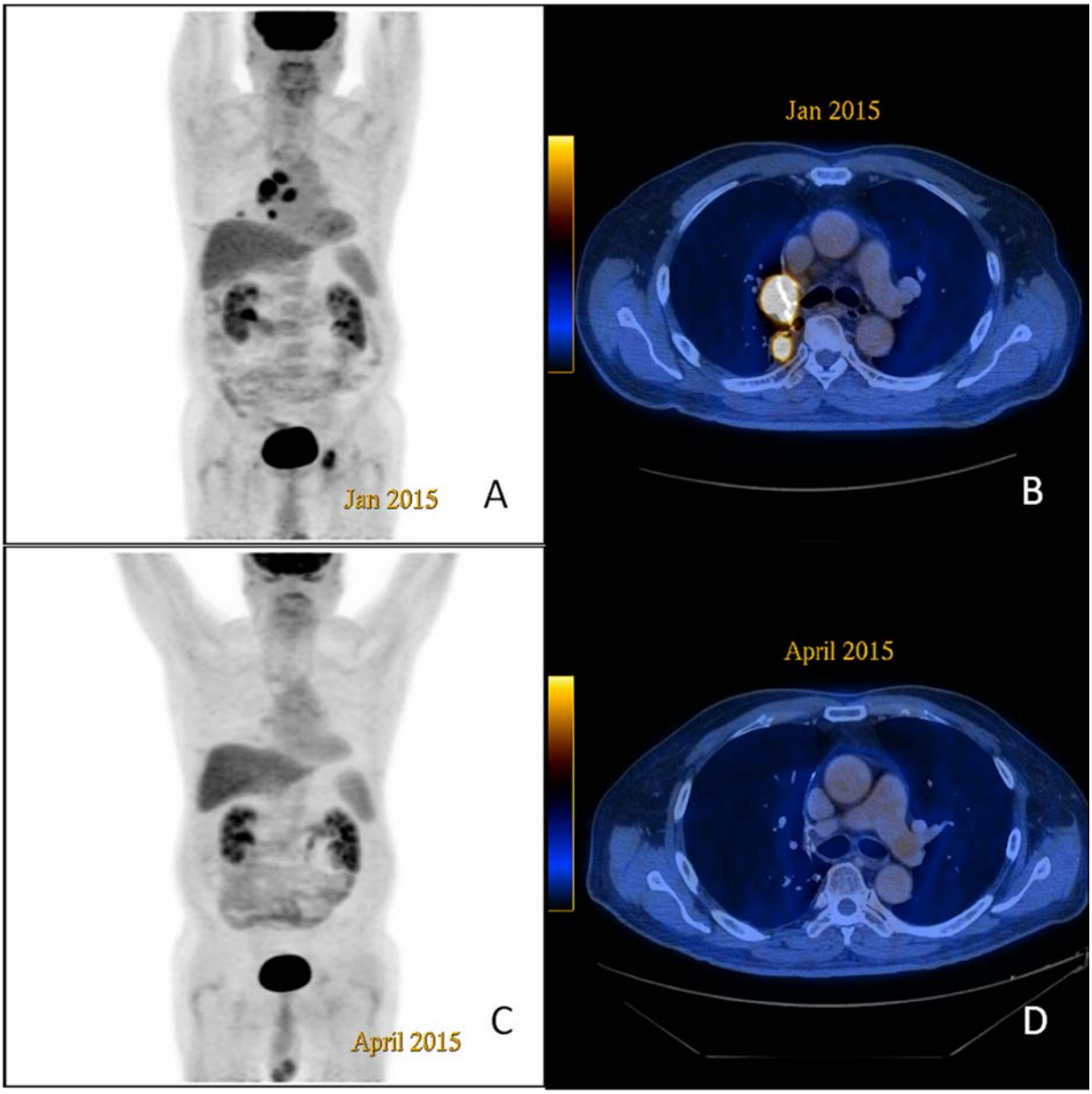

(A) ^{18}FDG PET MIP image shows hypermetabolic disease recurrence adjacent to previous surgical resection with hypermetabolic right mediastinal nodal metastases and solitary distant osseous metastasis in the posterior left acetabulum.
(B) Axial fused ^{18}FDG PET/CT image shows tumour recurrence adjacent to the surgical resection margin, 2.8 x 2.2 cm with SUVmax 9.1.
(C) ^{18}FDG PET MIP image shows complete metabolic treatment response in the tumour recurrence and metastases following 4 cycles of chemotherapy.
(D) Axial fused ^{18}FDG PET/CT image shows complete resolution of the tumour recurrence and nodal metastases following chemotherapy.

Fig. 4

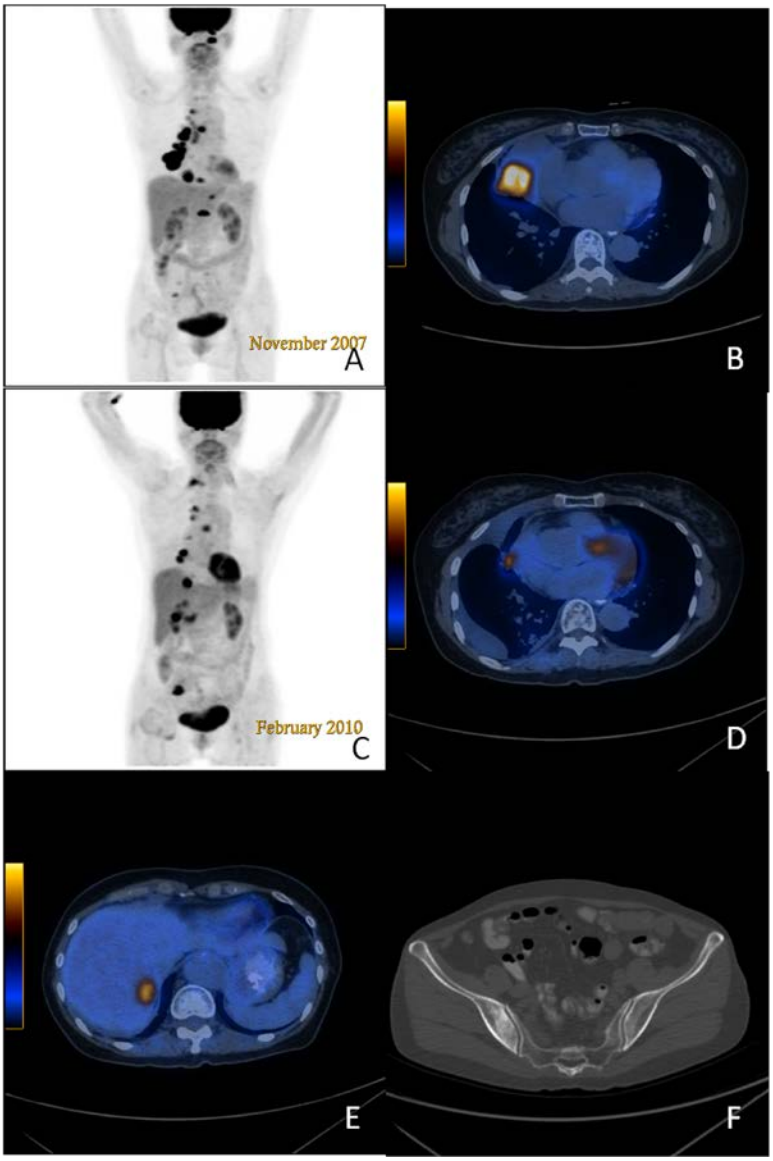

(A) ^{18}FDG PET/CT in November 2007: ^{18}FDG PET MIP image shows primary right middle lobe lung mass with mediastinal, right hilar and intra-abdominal nodal metastases.
(B) ^{18}FDG PET/CT in November 2007: Axial fused image shows right middle lobe tumour, which measures 4.5 x 3.5cm with SUVmax 12.5.
(C) ^{18}FDG PET/CT in February 2010: ^{18}FDG PET MIP image shows apart from local thoracic disease recurrences, there are new hepatic metastases and bony metastases.
(D) ^{18}FDG PET/CT in February 2010: Axial fused ^{18}FDG PET/CT image shows right middle lobe tumour recurrence, which measures 1.8 x 1.8cm with SUVmax 7.6.
(E) ^{18}FDG PET/CT in February 2010: Axial fused ^{18}FDG PET/CT image shows a hypermetabolic hepatic metastasis.
(F) ^{18}FDG PET/CT in February 2010: Axial CT shows right ilium sclerotic osseous metastasis.

Fig. 5

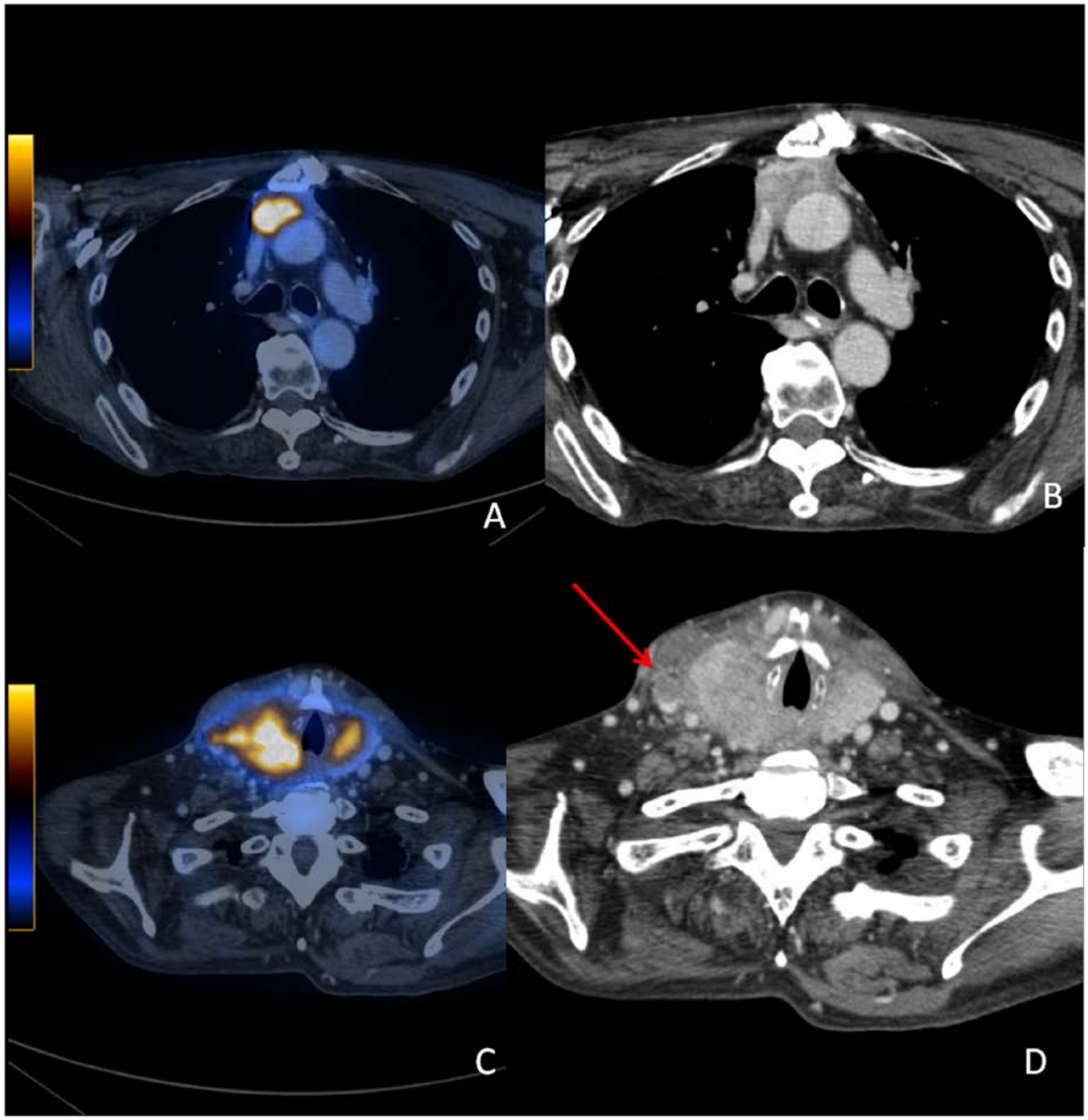

(A) Axial fused ^{18}FDG PET/CT image shows hypermetabolic anterior mediastinal mass, which measures 8.7 x 5.6 cm with heterogeneous ^{18}FDG uptake (SUVmax 14.9).
(B) Corresponding axial CT image shows the anterior mediastinal mass is partially encasing the superior vena cava and ascending aorta.
(C) Axial fused ^{18}FDG PET/CT image shows hypermetabolic tumour infiltration of both thyroid lobes.
(D) Corresponding axial CT image shows heterogeneous enhancement of the right thyroid lobe, local invasion into the adjacent soft tissue and tumour thrombus in the right jugular vein (arrow).

Fig. 6

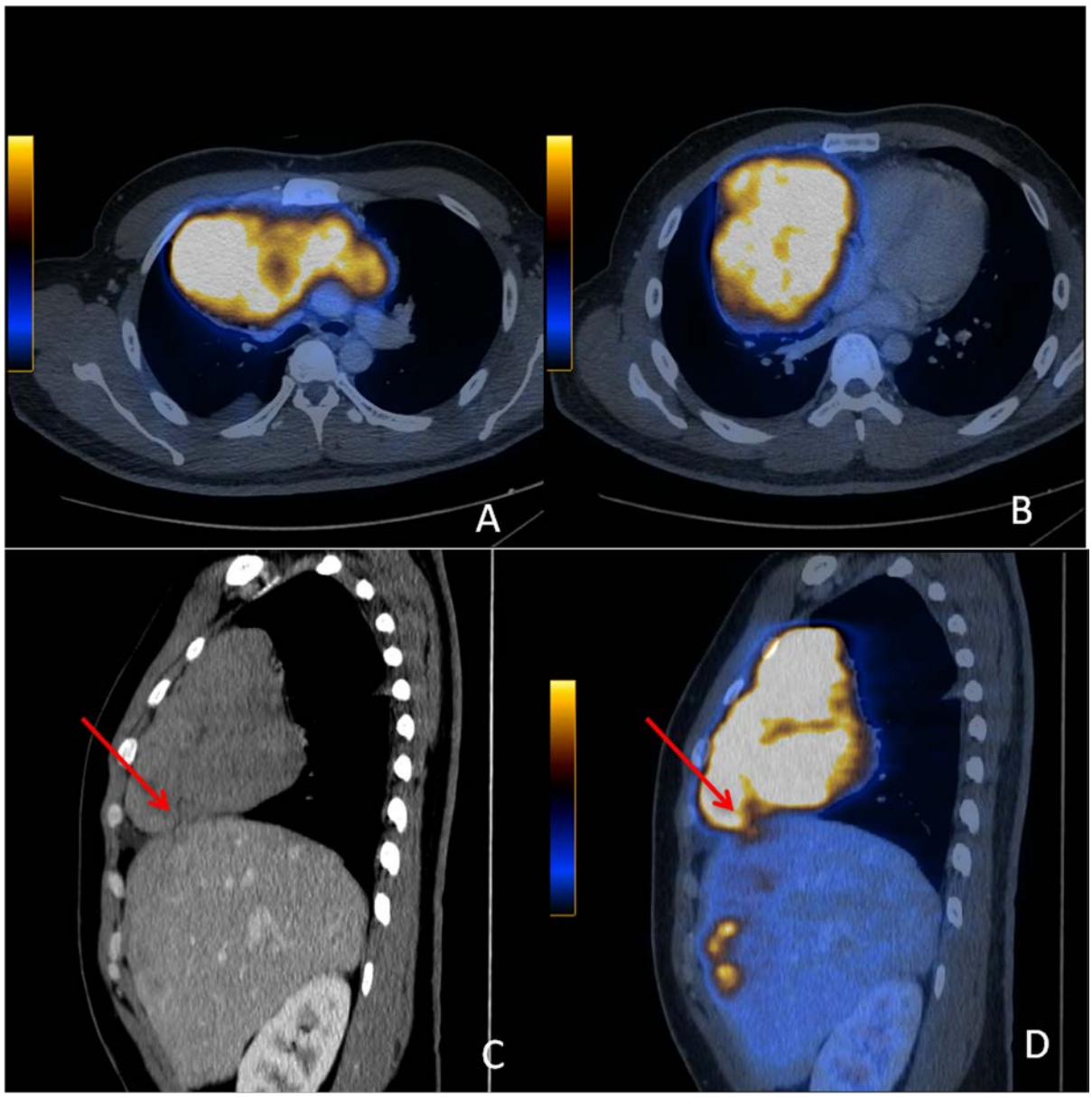

(A) Axial fused ^{18}FDG PET/CT image shows a large hypermetabolic anterior mediastinal mass, 14.4 x 10.7 cm with SUVmax 14.5, which is indistinguishable from malignant lymphoma and thymic carcinoma

(B) Axial fused ^{18}FDG PET/CT image shows the extension of the hypermetabolic anterior mediastinal mass into the right hemithorax.

(C) Sagittal CT image shows transcoelomic spread directly from mediastinum to liver (arrow).

(D) Sagittal fused ^{18}FDG PET/CT image shows the extension of ^{18}FDG uptake from mediastinum to the dome of the liver (arrow).

Fig. 7

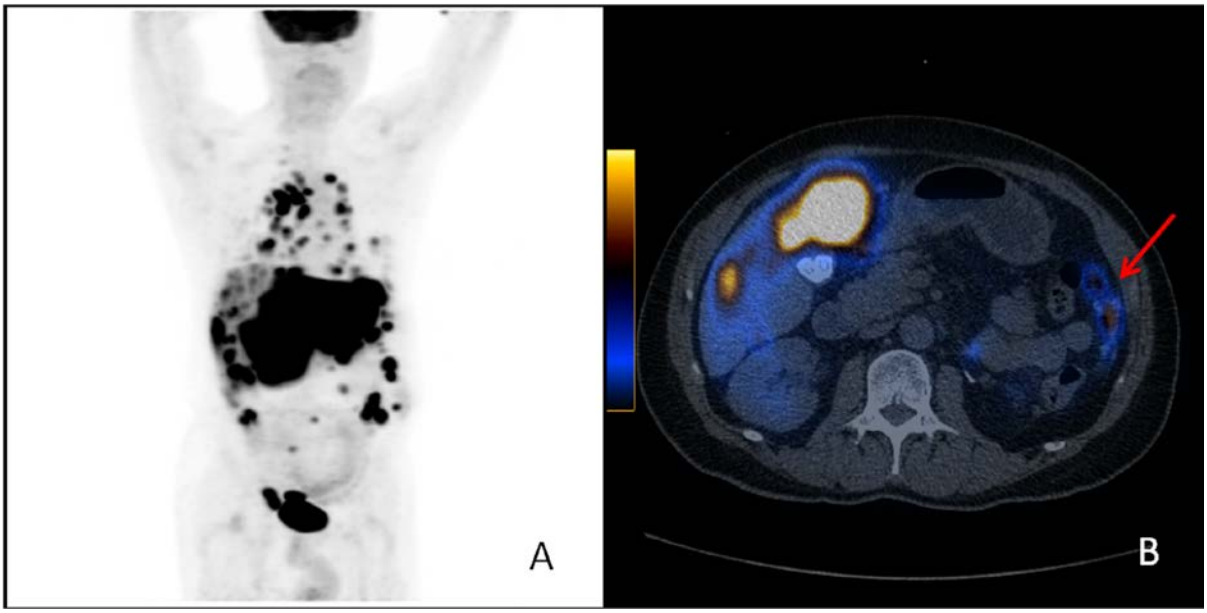

(A) ^{18}FDG PET MIP shows the presence of hypermetabolic multi-compartmental lymphadenopathy, lung, liver and intra-peritoneal metastases.
(B) Axial fused ^{18}FDG PET/CT image shows hypermetabolic hepatic metastases and peritoneal metastases in the left paracolic gutter (arrow).